THE POPULATION OF HELIUM-MERGER PROGENITORS: OBSERVATIONAL PREDICTIONS

Chris L. Fryer[1,2,3], Krzysztof Belczynski[4,5], Edo Berger[6], Christina Thöne[7], Carola Ellinger[8], Tomasz Bulik[4]

Draft version November 6, 2012

ABSTRACT

The helium-merger gamma-ray burst progenitor is produced by the rapid accretion onto a compact remnant (neutron star or black hole) when it undergoes a common envelope inspiral with its companion's helium core. This merger phase produces a very distinct environment around these outbursts and recent observations suggest that, in some cases, we are detecting the signatures of the past merger in the GRB afterglow. These observations allow us, for the first time, to study the specific features of the helium merger progenitor. In this paper, we couple population synthesis calculations to our current understanding of gamma-ray burst engines and common envelope evolution to make observational predictions for the helium-merger gamma-ray burst population. Many mergers do not produce GRB outbursts and we discuss the implications of these mergers with the broader population of astrophysical transients.

Subject headings: Supernovae: General, Stars: Neutron

1. INTRODUCTION

The black hole accretion disk gamma-ray burst (GRB) engine has become standard for long- and short-duration GRBs alike (Popham et al. 1999). For long-duration bursts, the most commonly-invoked progenitor is the collapse of a rapidly rotating massive star down to a black hole. But achieving the high angular momentum needed to produce a disk around the newly formed black hole has proved problematic and a number of progenitors have been invoked to provide these high angular momentum profiles (Fryer & Woosley 1998; Fryer et al. 1999a; Yoon & Langer 2005; Woosley & Heger 2006; Belczynski et al. 2007; Ivanova & Podsiadlowski 2003; Portegies-Zwart, Dewi, & Maccarone 2005; van den Heuvel & Yoon 2007; Fryer et al. 2007a; Podsiadlowski et al. 2010).

One such model invokes the merger of a compact remnant with its companion. As the compact remnant spirals into the center of the helium core of an evolved companion, the accretion rate can exceed $0.01 \, M_\odot \, s^{-1}$, enough to power a strong gamma-ray burst (Fryer & Woosley 1998). The basic idea behind this model is that as the compact remnant spirals into its companion, the orbital energy lost both spins up the helium core and ejects the hydrogen envelope. If the compact remnant is a neutron star, the rapid accretion in the inspiral is likely to cause it to collapse to a black

hole. In this manner, the helium merger model provides a natural way to ensure enough angular momentum to form a disk around a central black hole.

Simulations by Zhang & Fryer (2001) showed that the inspiral would produce both the high angular momenta and accretion rates needed to create a black hole accretion disk engine. Although there is some concern that helium mergers produce disks with too much angular momentum (DiMatteo et al. 2002), current analyses find this angular momentum is appropriate for accretion disk engines(Komissarov & Barkov 2009; Barkov & Komissarov 2011). The helium-merger model predicts a feature that may be observable in the resultant explosion: the existence of a shell (or torus) of merger-ejecta surrounding the burst.

Initially, Fryer & Woosley (1998) believed the helium merger model would be difficult to distinguish from normal GRBs because the ejecta from the common envelope phase would lie along the orbital plane (the same plane as the disk) and there would be very little interaction between the ejecta and the GRB jet. This picture changed with the observation of GRB121225, the so-called "Christmas Burst"(Thöne et al. 2011). This burst exhibited blackbody emission arguing for a compact progenitor ($\sim 10^{11}$ cm) followed by a second blackbody component with characteristic radius of $\sim 10^{14}$ cm. Simulations of the jet interactions with more realistic common envelope ejecta profiles (also based on recent simulations) found that the helium merger model could produce the thermal emission in this burst (Thöne et al. 2011). The X-ray Flare 060218 (and perhaps a few other low-redshift bursts) may have similar characteristics, suggesting that these helium merger events may be identifiable after all.

To truly compare these systems to the observed data, we must understand the entire population of compact merger events. In this paper, we undertake a series of population synthesis models studying the characteristics of compact merger events. Section 2 describes the population synthesis calculations and presents the basic results of these calculations: rates and characteristics of merging systems. In section 3, we analyze these results,

[1] CCS Division, Los Alamos National Laboratory, Los Alamos, NM 87545, USA
[2] Department of Physics, The University of Arizona, Tucson, AZ 85721, USA
[3] Department of Physics and Astronomy, The University of New Mexico, Albuquerque, NM 87131, USA
[4] Astronomical Observatory, University of Warsaw, Al. Ujazdowskie 4, 00-478 Warsaw, Poland
[5] Center for Gravitational Wave Astronomy, University of Texas at Brownsville, TX 78520, USA
[6] Harvard-Smithosonian Center for Astrophysics, 60 Garden Street, Cambridge, MA 02138, USA
[7] IAA-CSIC, Glorieta de la Astronomía s/n, 18008 Granada, Spain
[8] Department of Physics, University of Texas at Arlington, 502 Yates Street, Box 19059, Arlington, TX 76019, USA

making predictions for luminosities and ejecta positions for merger outbursts. We conclude with a discussion of the potential observational outcomes of this black hole accretion disk progenitor.

2. NEUTRON STAR MERGER POPULATIONS

2.1. *Population Synthesis Calculations*

To study the helium merger progenitor, we use the population synthesis code `StarTrack` to calculate the numbers and properties of merging systems. The full description of the code can be found in Belczynski, Kalogera, & Bulik (2002); Belczynski et al. (2008). The code utilizes a set of stellar models (Hurley, Pols, & Tout (2000); slightly modified from its original version) that allow for the evolution of stars at different metallicities. The model for compact object formation adopted in the code has been significantly revised (Dominik et al. 2012). During core collapse, fallback and direct BH formation is now accounted for (Fryer & Kalogera 2001) and the newly born objects receive natal kicks (Hobbs et al. 2005). The formation of low mass NSs through electron capture supernovae is also accounted for (e.g., Podsiadlowski et al. (2004)). Binary interactions are treated in detail, and the various physical processes have been calibrated using either results of detailed evolutionary calculations (e.g., Wellstein & Langer (1999) for mass transfer sequences), or specific sets of observations (e.g., Levine, Rappaport, & Zojcheski (2000) for tidal interactions). The mass loss prescription for winds in massive stars, the stellar binding energy used in common envelope evolution, and the compact remnant mass formation prescription have all been updated (Dominik et al. 2012).

2.2. *Rates*

In each calculation, we have evolved $N = 2 \times 10^5$ binaries with the primary mass range $M_1 = 5 - 150$ M$_\odot$ and secondary mass range $M_1 = 0.08 - 150$ M$_\odot$. The stars were evolved with solar metallicity ($Z = 0.02$). Each binary system is initiated by four parameters, which are assumed to be independent: the primary mass M_1 (the initially more massive component), the mass ratio $q = \frac{M_2}{M_1}$, where M_2 is the mass of the secondary, the semi-major axis a of the orbit, and the orbital eccentricity e.

For both, single stars and binary system primaries, we use the initial mass function adopted from Kroupa & Weidner (2003),

$$\Psi(M) \propto \begin{cases} M^{-1.3} & 0.08 \leq M < 0.5 \text{ M}_\odot \\ M^{-2.2} & 0.5 \leq M < 1.0 \text{ M}_\odot \\ M^{-\alpha_{\rm imf}} & 1.0 \leq M < 150 \text{ M}_\odot \end{cases} \quad (1)$$

where parameter $\alpha_{\rm imf} = 2.35 - 3.2$, with our standard choice of 2.7.

We adopt a flat mass ratio distribution that is consistent with the recent observational results (Kobulnicki, Fryer & Kiminki 2006),

$$\Phi(q) = 1 \quad (2)$$

in the range $q = 0 - 1$. Given value of the primary mass and the mass ratio, we obtain the mass of the secondary $M_2 = qM_1$.

TABLE 1
POPULATION SYNTHESIS MODELS

Model	λ_{CE}	Hertzprung Gap Fate[a]	Metallicity
Model1	physical λ[b]	CE formulae	solar
Model2	3×physical λ	CE forumulae	solar
Model3	constant $\lambda = 1$	CE formulae	solar
Model4	physical λ	HG always merges	solar
Model5	physical λ	CE formulae	10% solar
Model6	physical λ	HG always merges	10%solar

[a] Stars in the Hertzprung gap do not have strong entropy gradients dividing the helium core and hydrogen envelope. Without these sharp gradients, every CE phase will proceed through the merger with the helium core. We choose two fates: ignore this entropy argument ("CE formulae") or include this effect and assume on Hertzprung gap CE scenarios lead to a merged system ("HG always merges"). For more details, see Dominik et al. (2012).
[b] Physical λ corresponds to the Xu & Li (2010) used by Dominik et al. (2012).

The distribution of the initial binary separations is assumed to be flat in the logarithm (Abt 1983),

$$\Gamma(a) \propto \frac{1}{a}, \quad (3)$$

where a ranges from a minimum value, such that the primary fills at maximum 50% of its Roche lobe at ZAMS, up to 10^5 R$_\odot$.

We adopt the thermal-equilibrium eccentricity distribution for initial binaries,

$$\Xi(e) = 2e, \quad (4)$$

in the range $e = 0 - 1$ (e.g., Heggie 1975; Duquennoy & Mayor 1991).

We have evolved only binaries massive enough to potentially produce at least one compact object and therefore produce a helium merger. If we extend the evolved population to include the entire mass spectrum and if we include single stars as well (with binary fraction $f_{\rm bi} = 0.5$), each calculation with $\alpha_{\rm imf} = -2.7$ would correspond to a stellar mass formed in a starburst mass of 4.5×10^7 M$_\odot$.

Table 2 shows the total number of he-mergers produced using 2×10^5 binaries. The rates are divided into 3 categories: main-sequence merger and mergers with small, and large, helium core masses. These rates correspond to the rate per 4.5×10^7 M$_\odot$ of star forming mass. The number in parantheses show the number of the total systems produced because of neutron star kicks. Although kicks produce many of the merging systems (30%), kick-induced mergers account for a smaller fraction ($\sim$10%) of low-mass helium core mergers and almost nobe ($<$1%) of the massive helium mergers believed to be GRBs.

These rates can be folded with any desired star formation history to give actual time dependent helium merger rate in a given galaxy. Table 3 shows the merger rate per Myr in a Milky-Way massed galaxy as well as the volumetric (Gpc^{-3} yr^{-1}) rate. If we wish to compare to GRBs, a rough estimate of the rates should include a combination of solar and low metallicity rates (e.g. 50% each of Model 1 and Model 5 or 50% each of Model 4 and Model 6). The resultant rates predicted are 629, 857 Gpc^{-3} yr^{-1} for respective models assuming normal CE

TABLE 2
Merger Rates (per 4.5×10^7 M$_\odot$)

Model	He-Merger ($M_{\rm He} < 4.0 M_\odot$)	He-Merger Rate ($M_{\rm He} > 4.0 M_\odot$)	Main-Sequence Merger Rate
Model1	718(110)[a]	939(0)	579(175)
Model2	507(35)	406(0)	1267(411)
Model3	967(94)	227(3)	1566(478)
Model4	929(24)	1020(2)	580(175)
Model5	1505(1)	2019(9)	796(249)
Model6	1790(1)	3033(6)	755(262)

[a] The left number in each column denotes the total number of systems produced in each category. The numbers in parantheses show the number of these systems formed due to neutron star kicks.

TABLE 3
Merger Rates II (Myr^{-1}, Gpc^{-3} yr^{-1})

Model	He-Merger ($M_{\rm He} < 4.0 M_\odot$)	He-Merger Rate ($M_{\rm He} > 4.0 M_\odot$)	Main-Sequence Merger Rate
Model1	30.8(308.2)[a]	40.3(403.0)	24.9(248.5)
Model2	22.0(220.3)	17.6(176.4)	55.0(550.5)
Model3	43.2(431.5)	10.1(101.3)	69.9(69.9)
Model4	39.9(399.2)	43.8(438.3)	24.9(249.3)
Model5	63.7(636.7)	85.4(854.2)	33.7(336.8)
Model6	75.2(752.4)	127.5(1274.8)	31.7(317.3)

[a] The left number in each column denotes a rate per Milky-Way massed galaxy (Myr^{-1}). The numbers in parantheses show volumetric rate (Gpc^{-3} yr^{-1}).

formulae for Hertzsprung gap mergers versus immediate mergers for these Hertzsprung gap mergers.

The Fryer et al. (1999) Galactic rate for their standard model is $35\,\mathrm{Myr}^{-1}$, very close to our rate of high-mass helium cores. Such high rates mean that even if only 10% of these systems produce GRB jets, they can explain a large fraction of the GRB rates. The low-mass helium star merger and main-sequence merger rate is not significantly higher and, assuming these mergers produce peculiar supernovae, they can account for no more than 1% of all core-collapse sueprnovae.

Like long-duration GRBs, the delay time from star formation to merged event is limited to the stellar evolution time (in the he-merger case, it is the stellar evolution time of the companion star). For massive helium mergers, the merger occurs within $20\,\mathrm{Myr}$ of the initial star formation time (for main-sequence star mergers, the distribution can extend to $100\,\mathrm{Myr}$). These objects will likely trace star formation.

2.3. Mass and Orbital Separation Distributions

Our populations demonstrate that compact remnant mergers can occur for a wide range of star characteristics: mass, evolutionary phase and, hence, orbital separation at the time of the merger. In section 3, we will use these characteristics to determine observable features of these mergers. Before we do so, let's review the characteristics of these populations.

Figures 1,2 show the distribution of companion masses for 4 different merger populations: those with hydrogen cores merging through mass transfer, those with hydrogen cores merging when the compact remnant is kicked
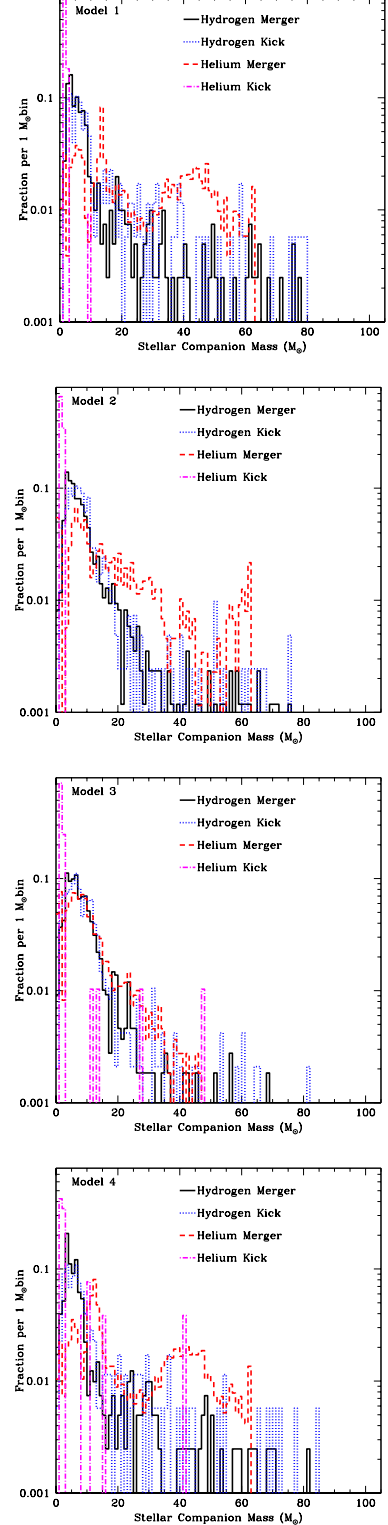

Fig. 1.— Companion star mass distribution for 4 different populations: those with hydrogen cores merging through mass transfer, those with hydrogen cores merging when the compact remnant is kicked into the companion, those with helium cores merging through mass transfer, and those with helium cores merging when the compact remnant is kicked into the companion. Except for helium merger systems (which have companion masses ranging up to $60\,\mathrm{M}_\odot$, often with a secondary peak at these high masses), most of the systems have companion masses peaking strongly at low masses.
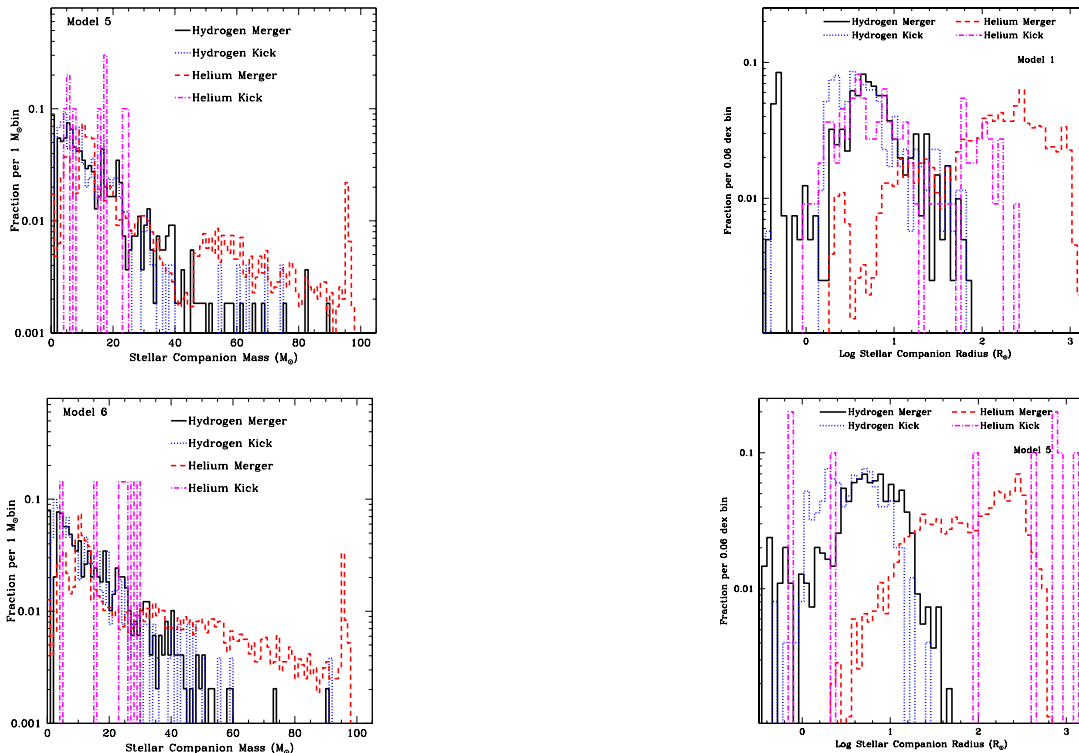
FIG. 2.— Companion star mass distribution for 4 different populations (see fig. 1). Note that for low metallicity systems, the helium merger population has a much broader high-mass tail, producing mergers with helium cores in excess of $90\,M_\odot$.

into the companion, those with helium cores merging through mass transfer, and those with helium cores merging when the compact remnant is kicked into the companion. As we might expect with our steep initial mass function, the companion masses are peaked to lower mass (below $20\,M_\odot$). However, the distribution is broad, extending beyond $60\,M_\odot$. He-merging systems have a secondary peak at higher masses and the most massive helium cores will come from this peak. For low-metallicity stars, this secondary peak occurs nearly at $90\,M_\odot$.

Similarly, the distribution of companion radii is extremely broad (Fig. 3). As expected, the evolved stars (with helium cores) can be much larger (up beyond 5 A.U.). The helium core sizes tend to lie in a narrow range between $0.5\text{-}3\,R_\odot$.

The wide variation in these systems will produce a wide variation in the observational features of these explosions.

3. OBSERVATIONAL COMPARISONS

The characteristics of the compact binaries (companion masses, evolutionary phases, radii and orbital separations) allow us to estimate both the explosion luminosities and spectral features.

3.1. *Luminosities*

For explosion luminosities, we will divide the discussion into two categories based on the accretion rate. If the system has a massive helium core ($> 4M_\odot$), the accretion is sufficient to power a strong black-hole accretion disk engine discussed in classical GRBs. In these cases, even the neutrin-annihilation powered engine may be strong.
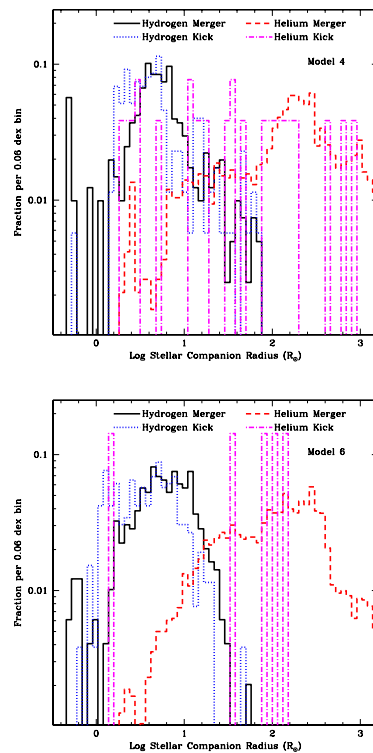

FIG. 3.— Companion star radius distribution for 4 different populations in Figure 1. The evolved stars (with helium cores) have much higher radii (up above 5 A.U.). Because there is very little variation between models, we show only 4 of our models.

These high accretion-rate systems fit the classic Helium Merger model proposed by Fryer & Woosley (1998). We then study low-mass helium core and hydrogen core systems.

3.1.1. *Massive Helium-core Merger: GRB-like*

Our population synthesis models predict a wide set of merging systems involving a compact remnant (neutron star or black hole) with its companion. As we showed in section 2.2, 8-50are mergers with evolved stars with helium core masses above $4\,M_\odot$. With a rate of 10-$120\,\mathrm{Myr}^{-1}$, mergers with massive helium cores can make up a significant fraction of our GRB population. In this section, we use our current understanding of disk-engine models to predict explosion luminosities from the helium core mass distribution.
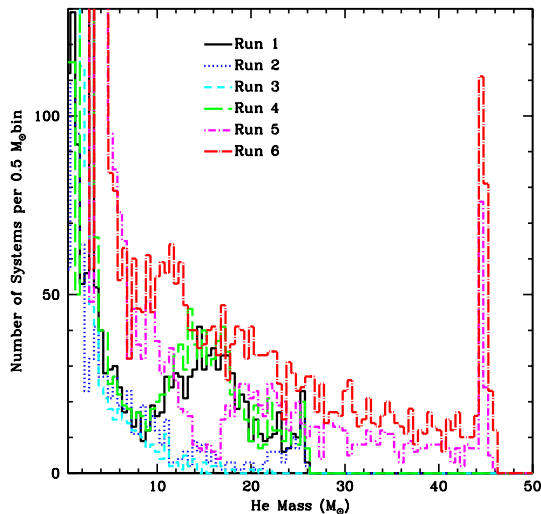

FIG. 4.— Mass distribution of helium cores in our population of he-mergers. The two largest peaks exist for low-mass helium cores: 1.4 and $3.4\,M_\odot$. But the distribution is widespread (half of all merging systems involve helium cores with masses above $4\,M_\odot$).

Zhang & Fryer (2001) studied the accretion onto a neutron star during an inspiral. They found that, the more massive the helium core, the higher the accretion rate (and, ultimately, the more energetic GRB explosion). Our population synthesis models provide us with the distributions of helium core masses at the onset of the merger is shown in Figure 4. Although the helium core masses peak at low masses, the distribution of helium core masses for solar metallicy models extends beyond $25\,M_\odot$ and roughly half of the systems have helium cores with masses above $4\,M_\odot$. At low metallicities, the maximum helium core mass extends from $25\,M_\odot$ up to $45\,M_\odot$.

We can estimate the accretion rate onto the compact remnant ($\dot{M}_{\mathrm{rem}}$):

$$\dot{M}_{\mathrm{rem}} = \eta M_{\mathrm{He}}/t_{\mathrm{free-fall}} =$$
$$\eta[2M_{\mathrm{He}}\sqrt{2.0G(M_{\mathrm{He}}+M_{\mathrm{rem}})}]/[\pi R_{\mathrm{He}}] \quad (5)$$

where $t_{\mathrm{free-fall}}$ is the free-fall timescale, M_{He}, R_{He} are the helium core mass and radius respectively, M_{rem} is the compact remnant mass and G is the gravitational

constant. The accretion rate is less than the typical free-fall time because the material has thermal pressure and considerable angular momentum. To account for this, we include an efficiency parameter η. Fitting to the Zhang & Fryer (2001) results, we find the value of η to be roughly 15%.
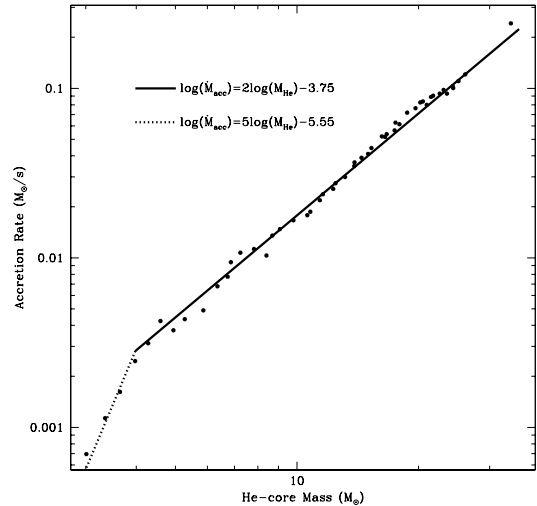

FIG. 5.— Average accretion rate as a function of helium core mass. The dots show results using the helium cores from the Woosley et al. (2002) models. The accretion rate data is fit by a 2-piece power law of the helium core mass. Below $4\,M_\odot$, the power increases dramatically, driving the accretion rate down significantly as the helium core mass decreases.

By using the helium core radii as a function of mass from the Woosley et al. (2002) pre-collapse helium cores, we derive an accretion rate as a function of helium core mass is shown in figure 5. These helium cores are evolved (at collapse), but their radii are not too different from the unevolved cores used by Zhang & Fryer (2001). This mass loss rate is fairly well fit by a 2-part power law:

$$\log(\dot{M}_{\mathrm{rem}}) = 2\log(M_{\mathrm{He}}) - 3.75 \text{ if } M_{\mathrm{He}} > 4.0$$
$$5\log(M_{\mathrm{He}}) - 5.55 \text{ otherwise.} \quad (6)$$

For helium cores with masses below $4\,M_\odot$, the accretion rate drops rapidly. These low-mass cores are less likely to drive strong explosions, and for the purposes of our discussion of helium mergers, we will focus on those helium cores with masses above $4\,M_\odot$.

Zhang & Fryer (2001) estimated the explosion luminosity as a function of accretion rate for a helium merger GRB assuming both the Blandford-Znajek (Blandford & Znajek 1977) and neutrino annihilation mechanisms. For neutrino annihilation, we use the formula from Zhang & Fryer(2001):

$$\log[L_\nu, \bar{\nu}(\mathrm{ergs}^{-1})] \approx 43.6 + 4.89\log[\dot{M}_{\mathrm{rem}}/(0.01M_\odot s^{-1})]$$
$$+3.4a_{\mathrm{rem}} \quad (7)$$

where $a_{\mathrm{rem}} \equiv (J_{\mathrm{rem}}c)/(GM_{\mathrm{rem}}^2)$, J_{rem} is the angular momentum of the remnant and c is the speed of light. Values of a_{rem} for these mergers tend to lie in the range of 0.75-0.95. We will assume 0.9 for our estimates. This estimate assumes a roughly $3\,M_\odot$ black hole which, for
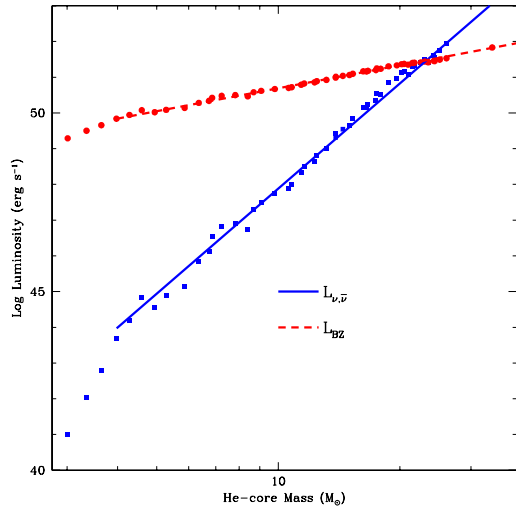
FIG. 6.— The luminosity versus helium core mass for our two power sources: neutrino annihilation ($L_{\nu,\bar{\nu}}$), Blandford-Znajek emission (L_{BZ}). The stronger dependence of neutrino annihilation on the density and temperature (and hence accretion rate) means that the luminosity from neutrino annihilation is extremely sensitive to the helium core mass.

the purposes of this study, is appropriate. However, other formulae exist that will produce different energy distributions, e.g. Zalamea & Beloborodov (2011). Our prescription produces a broader energy distribution than Zalamea & Beloborodov (2011) and, to demonstrate the range of energy distributions, we will focus on these formulae. However, one should bear in mind that the distribution of neutrino annihilation outbursts may be more narrow than predicted by our results.

The comparable equation for Blandford-Znajek emission is (Popham et al. 1999):

$$\log[L_{BZ}(\text{erg s}^{-1})] \approx 50.0 + 2\log[a_{rem}M_{rem}B_{mag}] \quad (8)$$

where B_{mag} is the magnetic field strength. As with Zhang & Fryer (2001), we will assume the magnetic energy density is equal to the kinetic energy density:

$$B^2 = 4\pi\rho v^2 \approx \dot{M}_{rem}c/r_g^2 \quad (9)$$

where we have approximated the density (ρ) and velocity (v) of the material using the values at the event horizon: $r_g = 2GM_{rem}/c^2$. Again, we set a_{rem} to 0.9 for our estimates. The corresponding luminosity for both these models as a function of helium core mass is shown in figure 6. Neutrino annihilation is much more sensitive to the helium core mass and leads to a broader spread of explosion energies.

These formulae allow us to estimate the luminosity of the outburst from our helium merger population. The distributions for both the neutrino annihilation and Blandford-Znajek models are shown in figure 7. As expected, the sensitivity of the neutrino annihilation emission model leads to a broad spectrum of explosion luminosities. Our simplified Blandford Znajek model predicts a relatively narrow range of luminosities from $10^{49} - 10^{51}$ ergs s^{-1}.

The merger process ejects the hydrogen atmosphere of the star in a shell of material with an density enhancement along the orbital plane. It was this shell that Thöne
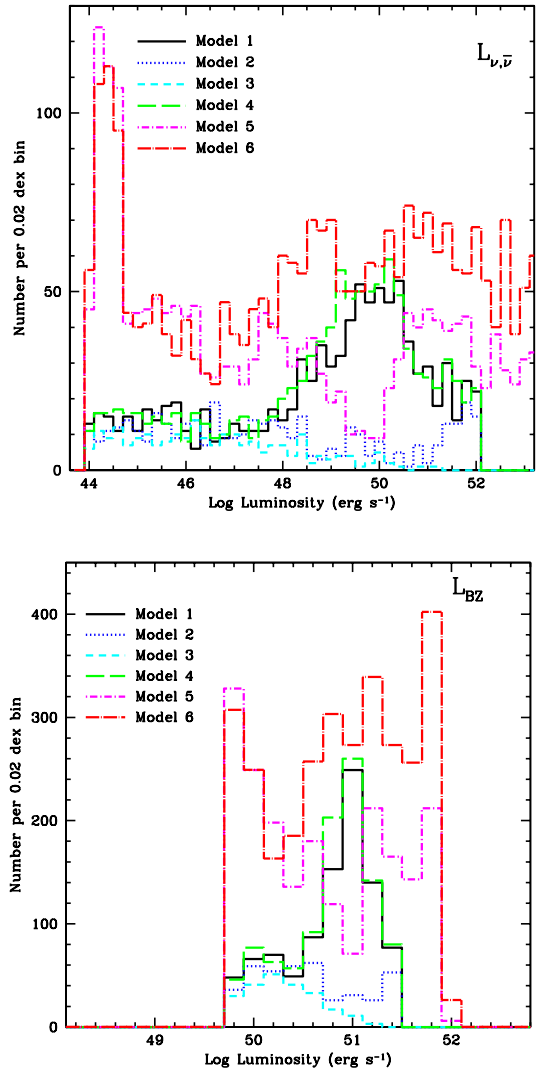

FIG. 7.— The distribution of luminosities from the helium mergers from our population synthesis calculations. The neutrino annihilation model's strong sensitivity on the helium core mass leads to a broad distribution in the explosion energies.

et al. (2011) exploited to explain the peculiar features of the Christmas burst. They argued that interactions of the jet with this shell produced the late-time, large radius blackbody emission. We estimate the outer extent of this shell using the same analysis of Thöne et al. (2011): assume the inspiral occurs in ∼3 orbits and the material ejected in this common envelope phase moves outward at the escape velocity. Although these two assumptions are not strictly true, we can not yet model this process exactly (e.g. Passey et al. 2011, Ivanova et al. 2012). These assumptions approximate the ultimate result within a factor of 2 in most cases. Using these assumptions, the corresponding distribution of shell positions for our populations are shown in figure 8.

Our population helium mergers predicts a range of luminosities versus maximum shell radii (Fig. 9). There is considerable scatter in the relationship between the outer shell radii and luminosity. But there is a trend that the most luminous explosions have the furthest shell distributions.
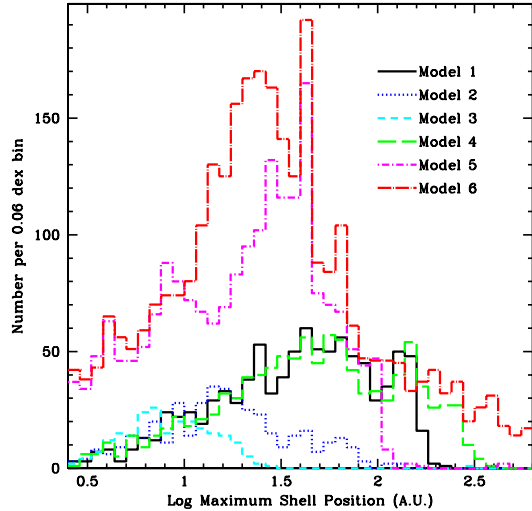
FIG. 8.— The distribution of outer positions of the helium merger ejecta from our population synthesis models.

3.1.2. *Supernova-like Explosions: Low-Mass Helium Cores and Main Sequence Mergers*

If the compact object merges with a lower-mass helium core or a main-sequence star, the accretion rate onto the remnant will be much lower. For these systems, the black hole accretion disk engine is unlikely to be valid and it is more difficult to produce even a rough estimate of the explosion energy.

Before the common envelope phase, many of our systems are likely to be X-ray binaries. At the onset of the common envelope phase, the X-ray binary can evolve, becoming more powerful. The system may even begin to produce strong jets. These so-called, micro-quasars, have been observed in numerous systems (see Mirabel 2007 for a review).

What happens as the compact remnant spirals into its companion is more difficult to determine. In these mergers, the accretion rate is slow enough that the neutron star may not initially collapse to form a black hole. The accretion rate remains high enough that any neutron star magnetic field is likely to be buried. Even without magnetic fields, these accretion events can produce explosions on par with normal supernova (Fryer et al. 2006a; Fryer 2009).

Presumably, once the compact remnant collapses to a black hole, the accretion disk will produce a jet. In these hydrogen or low-mass helium cores, the accretion rate is insufficient for the neutrino annihilation model to work, but we still do not understand the black hole accretion disk mechanism well enough to predict whether such systems will produce jets with explosions at GRB levels or at sub-supernova levels.

3.2. *Nucleosynthetic Yields*

Two sites have been identified in long-duration GRBs to produce ^{56}Ni: explosive nucleosynthesis in the shock (this shock burning is what produces the ^{56}Ni in supernovae), or disk-wind nucleosynthesis (Surman et al. 2006, 2011).

Explosive nucleosynthesis produces ^{56}Ni in the silicon and oxygen layers of an evolved core in normal super-
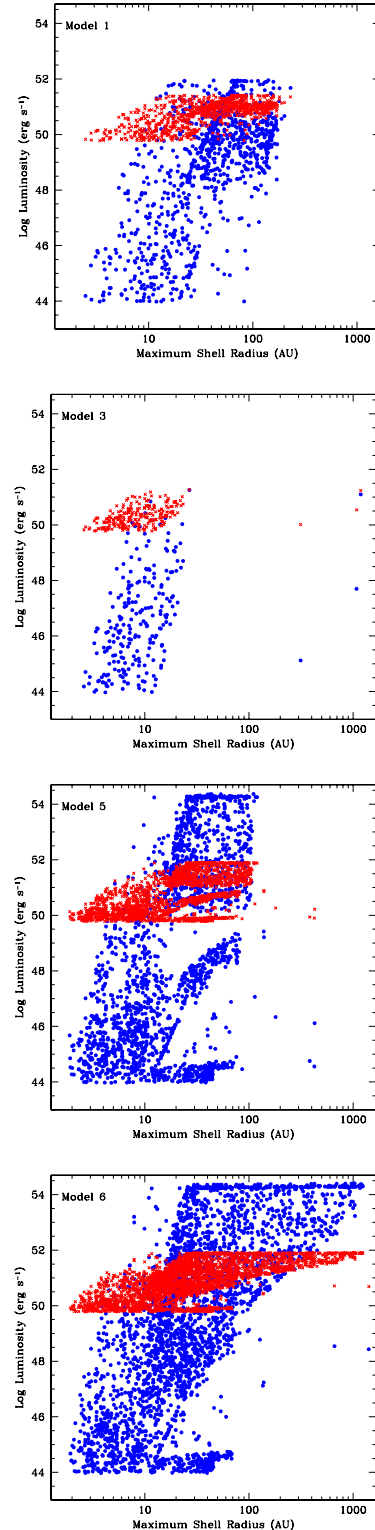

FIG. 9.— Luminosities versus outer shell radii for our helium merger population. Our Blandford-Znajek, magnetic field, engine (crosses) tends to produce stronger explosions in general, but the strongest explosion energies arise from our neutrino annihilation model (circles). The strongest energies tend to have the widest separations, but a there is considerable scatter in the maximum radius/luminosity relation.
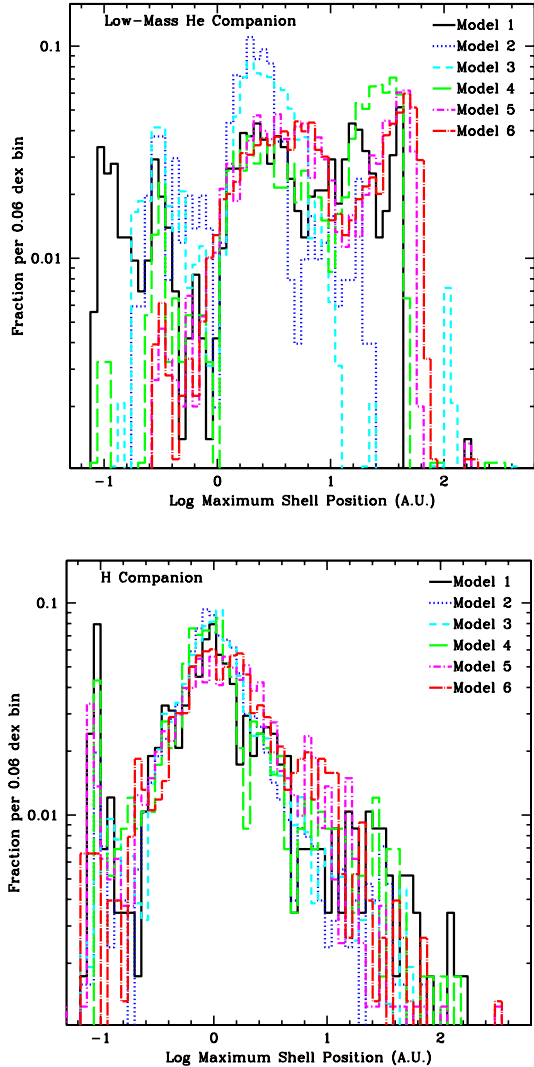
FIG. 10.— The distribution of outer positions of our low-mass helium cores and hydrogen stars. The distribution is much broader than the high-mass helium cores, with many more systems with quite low outer shell radii. The broad range of shell separations from these systems is in large part due to the fact that a sizable fraction of these systems (30% of hydrogen stars, 17% of low-mass helium stars) arise from systems where the compact remnant is kicked into its companion.

novae or classic collapsars. Without an evolved core, it is difficult for the helium merger model to produce significant ^{56}Ni from shock interactions. Unless considerable material is processed and ejected in the disk, very little ^{56}Ni is produced. Like the fallback GRBs discussed in Fryer, Hungerford & Young (2007b), these GRBs could produce low-nickel yield outbursts. Although this may not affect the peak of the light-curve (in most of these systems, shock heating dominates the light-curve at peak: Fryer et al. 2007b, Fryer et al. 2009), it does mean that if explosive nucleosynthesis is the dominant source of ^{56}Ni, these explosions will not have typical ^{56}Ni decay tails at late times.

However, if disk winds dominate the ^{56}Ni production, the nucleosynthetic yields of GRB-like he-mergers will be indistinguishable from collapsar long-duration GRBs.

3.3. *Spectra*

Contamination from the ejected hydrogen envelope is the strongest constraint for he-mergers. However, the hydrogen distribution in the helium merger model than in typical stellar envelopes. Even though the hydrogen remains within 10^{15} cm of the central engine, the distribution is very asymmetric. Passy et al. (2012) found that 90% of the mass ejected was distributed within 30° of the equator. It is more difficult to accurately describe the distribution of the remaining 10%. Combined with the fact that the explosion is also asymmetric, it is possible to sweep up very little mass.

How low must the swept-up hydrogen mass be? For symmetric explosions, Hachinger et al. (2012) found that roughly 0.1 solar masses of hydrogen could be hidden in the explosion. For asymmetric supernovae, this number may be a bit greater. This would require only 1-2% of the stellar-envelope hydrogen remain within the supernova opening angle (perhaps within 30° of the rotation axis).

To determine how well the low density funnel can focus the explosion, we have simulated using the SNSPH code (Fryer et al. 2006c; Ellinger et al. 2012) a 5.6×10^{51} erg explosion focused in a 30° wedge of a $25\,M_\odot$ where the density in this wedge is lowered by a factor of 100. The explosion at 0.47d is shown in figure 11. In this calculation, roughly $0.0001\,M_\odot$ of hydrogen is swept up in the explosion. This hydrogen mass is 3 orders of magnitude lower than typical type IIb supernovae and can easily be hidden in the spectra. This supernova would produce a Ib/c supernova.
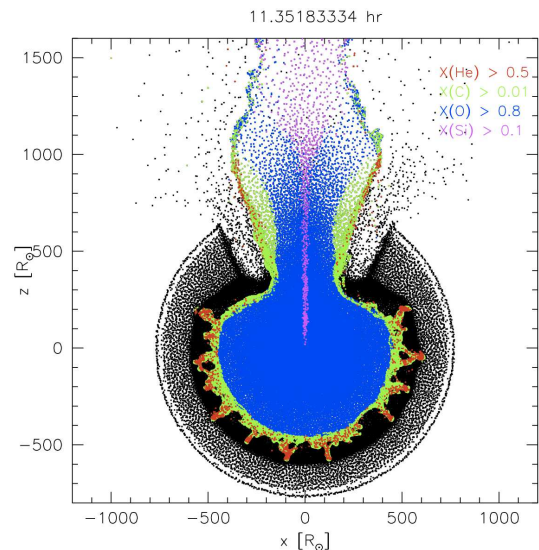

FIG. 11.— SNSPH particle positions for a 5.6×10^{51} erg explosion focused in a 30° wedge of a $25\,M_\odot$. The density in this wedge is lowered by a factor of 100 with respect to the rest of the star. Shading shows the different chemical abundances with black denoting hydrogen and lighter shades showing helium, carbon, oxygen and silicon abundances.

How much hydrogen is swept up (and whether or not we'll see it in the explosion) depends upon the details of the density profile set by the merger ejecta and the asymmetry in the explosion. For GRB-like jets expected from massive helium-core mergers, the amount swept up should not be detectable. But for main sequence stars,

the explosion may not be so jet-like, and the amount of hydrogen in the explosion could be large.

Finally, like with most collapsar progenitors, the helium in the ejecta must either be burned to C/O in the shock, or must be hidden in the supernova spectra. This remains one of the primary open problems with the Collapsar GRB model as well (Fryer et al. 2007a).

4. COMPARISON TO TRANSIENT POPULATIONS

We have shown that the rates of our massive he-core explosions are on par with the long-duration GRB rate, and the total he-merger and main-sequence merger rate is roughly 1% the supernova rate. For massive ($> 4\,M_\odot$) helium cores, energies can be as high as any black-hole accretion disk model. These models produce a range of hydrogen shells surrounding the star at 1-100 A.U. But to truly understand the nature of the explosions of these mergers requires a better understanding of the black-hole accretion disk engine. In this section, we review some of the possible outcomes of these objects.

4.1. *He-Mergers and GRBs*

We have shown that for a subclass of merging systems, the accretion rates onto the black hole can provide the energetics needed to drive a GRB outburst. In addition, the rate of this subclass is sufficient to explain GRBs. But can these mergers explain the full suite of GRB diagnostics.

Thöne et al. (2011) argued these mergers could fit a very peculiar subset of GRBs with an unusual optical counterpart. But can helium mergers explain a broader set of GRBs? One of the key constraints of long-duration GRB progenitors is the association of a particular subtype of supernova (Type Ic) with GRBs. The ^{56}Ni estimates for these supernovae tend to be higher than typical Ib/c supernovae with broader line profiles suggesting asymmetric explosions. Is it possible for the He-merger progenitor to reproduce this supernova/GRB association?

If the helium merger model can not satisfy these requirments, it may be limited to explaining only a few odd GRBs such as the Christmas burst. The shell position in the Christmas Burst ($\sim$10 A.U.) is characteristic of our he-merger predictions, but we expect a range shell positions from 1-100 A.U.

One feature of the helium merger model is that it typically has an order of magnitude higher angular momenta than the collapsar model. This leads to larger accretion disks with larger accretion times, although for the typical specific angular momenta of $10^{18}\,cm^2s^{-1}$, the accretion disk remains with 10^9 cm and may not produce drastically different characteristics than the Collapsar model.

At this point, our lack of understanding of the GRB engine makes it difficult to tie this difference in disk size to an observation. But as we better understand the engine, this difference may lead to observable consequences.

4.2. *Peculiar Supernovae*

If the explosion is asymmetric but there is too much hydrogen within the supernova explosion to produce a relativistic jet, helium helium mergers may produce asymmetric Ib/c supernovae or, if they sweep up more hydrogen, some fraction of the type IIb supernova population. These supernovae would be characterized by large asymmetries and, perhaps, larger ^{56}Ni yields.

Alternatively, if the disk explosion model produces more symmetric explosions, the helium merger model is more likely to produce a small subset of the type IIP supernovae and unless the ^{56}Ni yield is different, it may be difficult to uncover differences between he-merger outbursts from typical core-collapse explosions. Again, it is likely that these bursts exhibit stronger asymmetries than normal supernovae and evidence of these asymmetries may be the only other characteristic differentiating these explosions from normal type IIP supernovae.

Supernovae have been observed that may exhibit a recent shell ejection caused by a helium shell ejection (SN2011ht: Roming et al. 2012). Using the same analysis as section 3.1.1, we calculate the outer shell radii for both our low-mass helium cores and hydrogen stars 10. Note that the distribution has many more shells with outer radii below 1-2 A.U. The explosions from these mergers may, at peak, look very similar to comparable giant stars. A fraction (6% of hydrogen stars, 34% of low-mass helium cores) have outer shell radii beyond 10 A.U. that may produce the peculiar features of supernovae such as SN 2011ht. The broad range of shell separations from these systems is in large part due to the fact that a sizable fraction of these systems (30% of hydrogen stars, 17% of low-mass helium stars) arise from systems where the compact remnant is kicked into its companion.

4.3. *Radio Bursts*

If, in a GRB-like explosion, the jet sweeps up too much hydrogen to become relativistic, the engine does not produce much ^{56}Ni and supernova explosion is asymmetric (preventing it from sweeping up much mass), these explosions may produce optical weak, radio loud outbursts.

REFERENCES

Barkov, M.V., & Komissarov, S.S. 2011, MNRAS, 415, 944

Belczynski, K., Kalogera, V., & Bulik, T. 2002, ApJ, 572, 407

Belczynski, K., Bulik, T., Heger, A. & Fryer, C.L. 2007, ApJ, 664, 986

Belczynski, K., Kalogera, V., Rasio, F. A., Taam, R. E., Zezas, A., Bulik, T., Maccarone, T.J., & Ivanova, N. 2008, ApJS, 174, 223

Blandford, R.D., & Znajek, R.L. 1977, MNRAS, 179, 433

DiMatteo, T., Perna, R., & Naryan, R. 2002, ApJ, 579, 706

Dominik, M., Belczynski, K., Fryer, C. L., Holz, D. E., Berti, E., Bulik, T., Mandel, I., O'Shaughnessy, R. 2012, submitted to ApJ, astro-ph/1202.4901

Ellinger, C.I., Young, P.A., Fryer, C.L., & Rockefeller, G. 2012, ApJ, 755, 160

Fryer, C.L., & Woosley, S.E. 1998, ApJ, 502, L9

Fryer, C.L., Woosley, S., & Hartmann, D. 1999, ApJ, 526, 152

Fryer, C.L., & Kalogera, V. 2001, ApJ, 554, 548

Fryer, C.L., Rockefeller, G., Warren, M.S. 2006, ApJ, 643, 292

Fryer, C.L., Herwig, F., Hungerford, A.L., & Timmes, F.X. 2006, ApJ, 646, L131

Fryer, C.L., Young, P.A., & Hungerford, A.L. 2006, ApJ, 650, 1028

Fryer, C. L., et al. 2007, PASP, 119, 1211

Fryer, C.L., Hungerford, A.L., & Young, P.A. 2007, ApJ, 662, L55

Fryer, C.L. 2009, ApJ, 699, 409

Fryer, C.L., et al. 2009, ApJ, 707, 193

Hachinger, S., Mazzali, P.A., Taubenberger, S., Hillebrandt, W., Nomoto, K., Sauer, D.N. 2012, MNRAS, 422, 70

Hobbs, G., Lorimer, D. R., Lyne, A. G., & Kramer, M. 2005, MNRAS, 360, 974

Hurley, J.R., Pols, O.R., & Tout, C.A. 2000, MNRAS, 315, 543

Ivanova, N. & Podsiadlowski, P. 2003, in From Twilight to Highlight: The Physics of Supernovae, ed. W. Hillebrandt & B. Leibundgut (Berlin: Springer), 19

Komissarov, S.S. & Barkov, M.V. 2009, MNRAS, 397, 1153

Levine, A. M., Rappaport, S. A., & Zojcheski, G. 2000, ApJ, 541, 194

Mirabel, I.F. 2007, Comptes Rendus - Physique, 8, 7

Passy, J.-C., De Marco, O., Fryer, C.L., Herwig, F., Diehl, S., Oishi, J.S., Mac Low, M.-M., Bryan, G.L. & Rockefeller, G. 2012, ApJ, 744, 52

Podsiadlowski, P., Langer, N., Poelerands, A.J.T., Rappaport, S. Heger, A., & Pfahl, E. 2004, ApJ, 612, 1044

Podsiadlowski, P., Ivanova, N., Justham, S., Rappaport, S. 2010, MNRAS, 406, 840

Popham, R., Woosley, S.E., & Fryer, C.L. 1999, ApJ, 518, 356

Portegies-Zwart, S.F., Dewi, J., & Maccarone, T. 2005, Ap&SS, 300, 247

Roming, P.W.A., et al. 2012, ApJ, in press

Surman, R., McLaughlin, G.C. & Hix, W.R. 2006, ApJ, 643, 1057

Surman, R., McLaughlin, G.C. & Sabbatino, N. 2011, ApJ, 743, 155

Thone, C.C., et. al. 2011, Nature, 480, 72

van den Heuvel, E.P.J., & Yoon, S.-C. 2007, Ap&SS, 311, 177

Wellstein, S., & Langer, N. 1999, A&A, 350, 148

Woosley, S.E., Heger, A., Weaver, T.A., 2002, Rev. Mod. Phys., 74, 1015

Woosley, S.E. & Heger, A., ApJ, 637, 914

Xu, X.-J., & Li, X.-D. 2010, ApJ, 716, 114

Yoon, S.-C., & Langer, N. 2005, A&A, 443, 643

Zalamea, I., Beloborodov, A.M. MNRAS, 410, 2302

Zhang, W., & Fryer, C.L. 2001, ApJ, 550, 357